Opportunities of diagnostic imaging in monitoring the radiosurgery treatment for uveal melanoma

T.M. Babkina,[1] Dr Sc (Med), Prof.; **N.Iu. Spizhenko,**[2] Cand Sc (Med);
S.V. Valchishin,[2] Roentgenologist, MD; **I.N. Dykan,**[3] Dr Sc (Med), Prof.; **N.N. Kolotilov,**[3] Dr Sc (Biol)

[1] Shupik National Medical Academy of Postgraduate Education;
Kyiv (Ukraine)

[2] Spizhenko Medical Center LLC, Spizhenko Clinic™;
Kyiv (Ukraine)

[2] Institute for Nuclear Medicine and Diagnostic Imaging, NAMS of Ukraine;
Kyiv (Ukraine)

E-mail: tbabkina@ukr.net

Key words:
uveal melanoma, CT, MRI, stereotactic radiosurgery

Background: Uveal melanoma (UM) is a primary choroidal tumor of neuroectodermal origin with a high malignant potential. Organ-preserving stereotactic radiosurgery (SRS) treatment strategies can be used for patients with UM.

Purpose: To assess the potential of diagnostic imaging methods, computed tomography (CT) and magnetic resonance imaging (MRI), for the monitoring of SRS treatment outcomes for UM.

Methods: Twenty-six patients with UM (age, 27 years to 68 years) were involved in this study and underwent an examination. The uveal melanomas were classified as per the classification system by Shields. A standard bolus protocol with iodine-containing contrast agent (Ultravist) was used to perform CT imaging on an Activion TSX-031A Multislice CT Scanner. A standard brain MRI protocol (T1, T2, FLAIR, T1 Fsat, T2 Fsat, Short 3D 2mm T1) with non-ionic paramagnetic contrast medium (Omniscan™) was used to perform diffusion-weighted MRI and obtain apparent diffusion coefficient (ADC) values on a 1.5T Vantage Atlas MRI system. The G4 Cyberknife System was used to perform SRS treatment for UM with the clinical target volume coverage of 99.9%.

Results: Post-SRS changes in semiological elements in CT and MRI images were examined. Our imaging monitoring of patients with UM showed that UM ADC values substantially increased as early as month 1 or month 2 after SRS (whereas tumor tissue volumes decreased only 6 months after SRS). Thus, in small, medium-size and large tumors, UM ADC values increased by 18.1%, 20.0%, and 35.7%, respectively, at 1-2 months, and by 41.9%, 38.8%, and 64.3%, respectively, at 11-12 months.

Conclusion: CT and MRI are diagnostic imaging modalities provide valuable information in monitoring patients with UM. Diffusion-weighted MRI provides qualitative and quantitative characteristics of post-SRS changes in tumor process.

Introduction

In 1583, a German itinerant barber-surgeon, George Bartisch, was the first to describe uveal melanoma (UM) [1]. A French doctor and anatomist, René-Théophile-Hyacinthe Laennec, coined the term melanoma and provided a more detailed description of the clinical entity in 1819 [1]. Uveal melanoma is a slowly progressive primary choroidal malignancy of neuroectodermal origin [2, 3]; it is one of the most common primary malignant intraocular tumors in adults [4].

In addition, it is the second most common melanoma in adults after skin melanoma [3, 4]. Uveal melanoma accounts for about 12-15% of all melanoma cases and 85-90% of all intraocular neoplasm cases [4], and 10-year mortality rate increases with age [5]. In Europe, standardized incidence rates were found to increase from south to north across registries, from a minimum of <2 per million in registries of Spain and southern Italy up to >8 per million in Norway and Denmark [5]. Incidence rates are highest at ages 50 to 60 [2, 3]. The disease is somewhat

more common among women than men, by a ratio of approximately 1.32:1 [4]. Unilateral uveal melanoma is far more common than bilateral [2, 4]. Since conventional diagnostic techniques for UM fail to provide convincing evidence related to the location, nature of growth pattern, and cancerous growth from the eye, modern diagnostic imaging modalities (e.g., computed tomography (CT) and magnetic resonance imaging (MRI)) [2, 4, 6] should be used for this purpose. Advances in radiation treatment contributed to the introduction of stereotactic radiosurgery (SRS) into clinical practice, allowing for organ-preserving treatment strategies in patients with different stages of UM [7-10]. Since research has shown SRS treatment for UM with a protrusion measuring 10-12 mm (and even more in some cases) to be at least as beneficial as enucleation with

regard to metastasis rate and survival rate [9, 10], SRS treatment is commonly performed in these cases.

The purpose of this study was to assess the potential of diagnostic imaging methods, computed tomography (CT) and magnetic resonance imaging (MRI), for the monitoring of SRS treatment outcomes for UM.

Material and Methods

Twenty-six patients with UM (age, 27 years to 68 years; mean age, 53.4 ± 11.8 years) were involved in this study and underwent an examination. The uveal melanomas were classified as per the classification system by Shields [5] (Table 1).

A standard bolus protocol with iodine-containing contrast agent (Ultravist) was used to perform CT imaging on an Activion TSX-031A Multislice CT Scanner (Toshiba Medical Systems Corp., Tochigi, Japan). A standard brain MRI protocol (T1, T2, FLAIR, T1 Fsat, T2 Fsat, Short 3D 2mm T1) with non-ionic paramagnetic contrast medium [Omniscan™; GE Health Care, Oslo, Norway]) was used to perform diffusion-weighted MRI and obtain apparent diffusion coefficient (ADC) values on a 1.5T Vantage Atlas MRI system (Toshiba) at 3, 6, 9 and 12 months after SRS treatment for UM. Diffusion-weighted MRI techniques characterize the diffusive motion of water molecules in tissues [11]. The diffusion-weighted imaging (DWI) methodology applies a fat-suppressed spin-echo T2 weighted sequence with two extra gradient pulses. The degree of signal attenuation is proportional to the strength of the diffusion weighting which is denoted by a "b-value", a factor that is dependent on gradient length, amplitude and the spacing between them. The b-value can be adjusted and is usually within the range of 0-1.500 s/mm2. If the b-value is equal to 0 s/mm2, the image obtained practically cannot be distinguished from a T2-weighted and fat-suppressed image due to the absence of contribution of the diffusion weighting [11]. We used the b-value of 800 s/mm2, as per recommendations of [10, 12], since their preliminary evaluation on UM patients showed that a diffusion weighting of b = 1000 s/mm2, commonly used for neuro-imaging, resulted in a too strong attenuation of the signal from the tumor.

The G4 Cyberknife System was used to perform SRS treatment for UM with the clinical target volume (CTV) coverage of 99.9%.

SRS technique

A custom immobilizing mask was fabricated. The affected eye was immobilized by retrobulbar blockade through regional anesthesia, usually with lidocain or bupivacaine. CT scan was performed using 1–1.5 mm slices. Thereafter, MRI with intravenous contrast was performed. This allowed us to determine the amount of radiation to be delivered, and to develop the treatment plan. The tumor was delineated in axial planes (Fig. 1) in a way protecting the critical structures of the eye like the cornea, lens, macula lutea, optic disc and chiasm. The mean calculated tumor dose was 20.3 Gy ±2 Gy.

The mean follow-up period was 26.4 months.

Study protocol followed the guidelines of the Helsinki Declaration. Written informed consent was obtained from each patient before the study.

Variation statistics was applied for statistical analysis. Student t-test was used for paired comparison of mean values with the level of significance set at $p < 0.01$.

Results

On MRI, uveal melanomas appeared isointense and hyperintense in T1W images in 9/26 cases (34.6%) and 17/26 cases (65.4%), respectively, and hypointense in T2W images in all 26 cases (100%). After contrast material injection, tumor signal intensity increased in T1W images in all 26 cases (100%). In addition, tumor signal intensity increased in diffusion-weighted images, with the tumor showing restricted diffusion in the ADC map (Figs. 2-5).

Diffusion-weighted MRI is a quantitative technique for assessing the diffusion in the volume of interest, and does not provide for acquiring detailed anatomical images. Therefore, it may serve as an auxiliary tool for imaging functional changes in tissues, and should be used only for primary diagnosis, and only in combination with T1W images or CT images [6, 11].

Semiological elements in diffusion-weighted images and ADC of any tissue are qualitative and quantitative characteristics of tissue cellularity and cell destruction [11, 13]: the ADC in biologic tissue is inversely correlated to the tissue cellularity. Naturally, the loss of cell membrane integrity, tumor cell destruction, and UM radionecrosis are accompanied by an increase in the ADC (Table 2).

The relationship between tissue histology and ADC is rather intricate. Diffusion of water molecules in human tissues cannot be isotropic due to a number of space-related limitations (hydrophobic phospholipids of cell membranes and organelles, organelles and their density, intercellular space dimensions, and densities of cells of such and such tissues). High tissue cellularity and small intercellular space result in decreased diffusion [10, 11].

Although no calibration standard is available for ADC measurement, aqueous solutions of sodium chloride and acellular gelatinous gels with naturally high ADC values might be used for this purpose. Vitreous was used as calibration standard in vivo for ADC assessment in the volume of interest. In the current study, vitreous ADC values ranged from 2.67×10^{-3} mm2/s to 2.84×10^{-3} mm2/s; these values did not depend on the size of uveal melanoma tumors. Human vitreous is considered as a specialized connective tissue represented both by cell lineages varying in origin and function (hyalocytes located mostly at the vitreous periphery) and intercellular substance composed of a gel-like substance (with water content as high as 99%) with immersed collagen fibrils of the macromolecular scaffold. We found it reasonable to compare our baseline ADC values (1.05×10^{-3} mm2/s to 0.56×10^{-3} mm2/s) for tumor tissue in uveal melanomas varying in size with ADC values for low-density vitreous cell structure reported by others [10, 12, 14-16].

In the study by Kamrava and colleagues [17], mean uveal melanoma ADC was $(1.07 \pm 0.27) \times 10^{-3}$ mm2/s, which is comparable with our findings. Increased restricted diffusion in tumor tissue is related to high nucleocytoplasmic ratio in this tissue and densely packed cells with high-density hydrophobic membranes, with diffusion-weighted MRI showing a hyperintense structure of the tumor.

Our MRI monitoring of patients with UM showed that UM ADC values substantially increased as early as month 1 or month 2 after SRS (whereas tumor tissue volumes decreased only 6 months after SRS). Thus, in small, medium-size and large tumors, UM ADC values increased by 18.1%, 20.0%, and 35.7 %, respectively, at 1-2 months, and by 41.9%, 38.8%, and 64.3%, respectively, at 11-12 months. An increase in UM ADC values with time after SRS can be considered as evidence of necrosis and decrease in density in tumor cells. No MRI evidence of local UM recurrence was observed in patients during follow-up. A decrease in UM ADC value has been reported [17] as a criterion for local tumor recurrence.

On CT (Fig. 4), the tumor is located posterior to the ocular equator and exhibits a homogeneous hyperdense and well-delineated structure with an even contour which appears adjacent to the sclerouveal rim and spreads to the vitreous. Occurrence of a diffuse surface on CT is evidence of the presence of exudate. On post-contrast images, large tumors exhibit a heterogeneous structure resulting from necrosis and/or hemorrhage.

Conclusion

The use of imaging techniques (CT and MRI) in UM treatment monitoring after SRS enables identifying not only the qualitative but also the quantitative changes that evidence tumor progression or regression. We believe that ADC values can be used for predicting (a) the degree of malignancy of a neoplasm and (b) tumor tissue response to treatment. It is important that UM ADC values were found to increase (by 18.1% to 35.7%) as early as month 1 or 2 after SRS, evidencing tumor tissue regression, whereas the characteristics relevant to tumor dimensions and structure appeared to change at month 6 or later. CT- and MRI-guided precise irradiation of tumor tissue with minimum irradiation of the critical structures, particularly in the course of stereotactic radiosurgery, would improve the outcomes and quality of life of patients with uveal melanoma.

References

1. Char DH. History of ocular oncology. Ophthalmology. 1996 Aug;103(8 Suppl):S96-101.
2. Shirina TV. [Prognosis for survival at late time points after treatment for uveal melanoma]. [Abstract of Cand Sc (Med) Thesis]. Moscow: Helmholtz Research Institute of Eye Diseases; 2013. Russian.
3. Afshar AR, Damato BE. Uveal melanoma: Evidence for efficacy of therapy. Int Ophthalmol Clin. 2015 Winter;55(1):23-43. doi: 10.1097/IIO.0000000000000053.
4. Avakian KV. [Early diagnosis of metastatic disease in uveal melanoma]. [Cand Sc (Med) Thesis]. Moscow: Helmholtz Research Institute of Eye Diseases; 2018. Russian.
5. Metastasis of uveal melanoma millimeter-by-millimeter in 8033 consecutive eyes. Shields CL, Furuta M, Thangappan A, et al. Arch Ophthalmol. 2009 Aug;127(8):989-98. doi: 10.1001/archophthalmol.2009.208.
6. Beenakker J-WM, Ferreira TA, Doemarwoto KP, et al. Clinical evaluation of ultra-high-field MRI for three-dimensional visualisation of tumour size in uveal melanoma patients, with direct relevance to treatment planning. MAGMA. 2016 Jun;29(3):571-7. doi: 10.1007/s10334-016-0529-4.
7. Vazhenin AV, Panova IE, Semionova LE. [Our first experience of treating choroidal melanoma with the use of Cyber Knife]. Sibirskii onkologicheskii zhurnal. 2012;1(49):48-50. Russian.
8. Zabelin MV, Klimanov VA, Galiautdinova ZhZh. [Proton radiation therapy: clinical application opportunities and research prospects]. Issledovaniia i praktika v meditsine. 2018;(1):82-95. DOI: 10.17709/2409-2231-2018-5-1-10. Russian.
9. Iarovoi AA, Golanov AV, Il'ialov SR. [CyberKnife stereotactic surgery as an alternative to enucleation in patients with uveal melanoma]. Ophthalmosurgery. 2014;(2):74-80. Russian.
10. Foti PV, Longo A, Reibaldi M, et al. Uveal melanoma: Quantitative evaluation of diffusion-weighted MR imaging in the response assessment after proton-beam therapy, long-term follow-up. Radiol Med. 2017 Feb;122(2):131-9. doi: 10.1007/s11547-016-0697-3.
11. Ternovoy NK, Kolotilov NN, Tuz EV, Drobotun OV, Ulyanchich NV. Quantifiable tumor diffusion coefficient (overview and own data). Luchevaia diagnostika, luchevaia terapiia. 2018;(3):70-6.
12. Ferreira TA, Saraiva P, Genders SW, et al. CT and MR imaging of orbital inflammation. Neuroradiology. 2018 Dec;60(12):1253-1266. doi: 10.1007/s00234-018-2103-4.
13. Pulido JS, Campeau NG, Klotz E. Correlation of histological findings from a large ciliochoroidal melanoma with CT perfusion and 3T MRI dynamic enhancement studies. Clin Ophthalmol. 2008 Jun;2(2):275-81.
14. Ferreira TA, Grech Fonk L, Jaarsma-Coes MG, et al. MRI of Uveal Melanoma. Cancers (Basel). 2019 Mar 17;11(3). doi: 10.3390/cancers11030377.
15. Jaarsma-Coes MG, van Haren GR, Ferreira TA, et al. MR-imaging enables accurate diagnosis and follow-up in uveal melanoma patients after vitrectomy. Melanoma Res. 2019 Jan 16. doi: 10.1097/CMR.0000000000000568.
16. Jiang X, Asbach P, Willerding G. Dynamic contrast-enhanced MRI of ocular melanoma. Melanoma Res. 2015 Apr;25(2):149-56. doi: 10.1097/CMR.0000000000000142.
17. Kamrava M,. Sepahdari AR, Leu K. Quantitative multiparametric MRI in uveal melanoma: Increased tumor permeability may predict monosomy 3. Neuroradiology. 2015 Aug;57(8):833-40. doi: 10.1007/s00234-015-1546-0.

Table 1. Tumor size distribution for patients with uveal melanoma

Uveal melanoma size	Thickness, mm	Diameter, mm	Patients, No (%)
Small	≤ 3.0	≤ 10.0	14 (53.8)
Medium	3.1—5.0	10.1—15.0	8 (30.8)
Large	≥ 5.1	≥ 15.0	4 (15.4)

Table 2. Apparent diffusion coefficient (ADC) values (M±m x 10^{-3} mm^2/s) for the tumor and vitreous before and after stereotactic radiosurgery for uveal melanoma

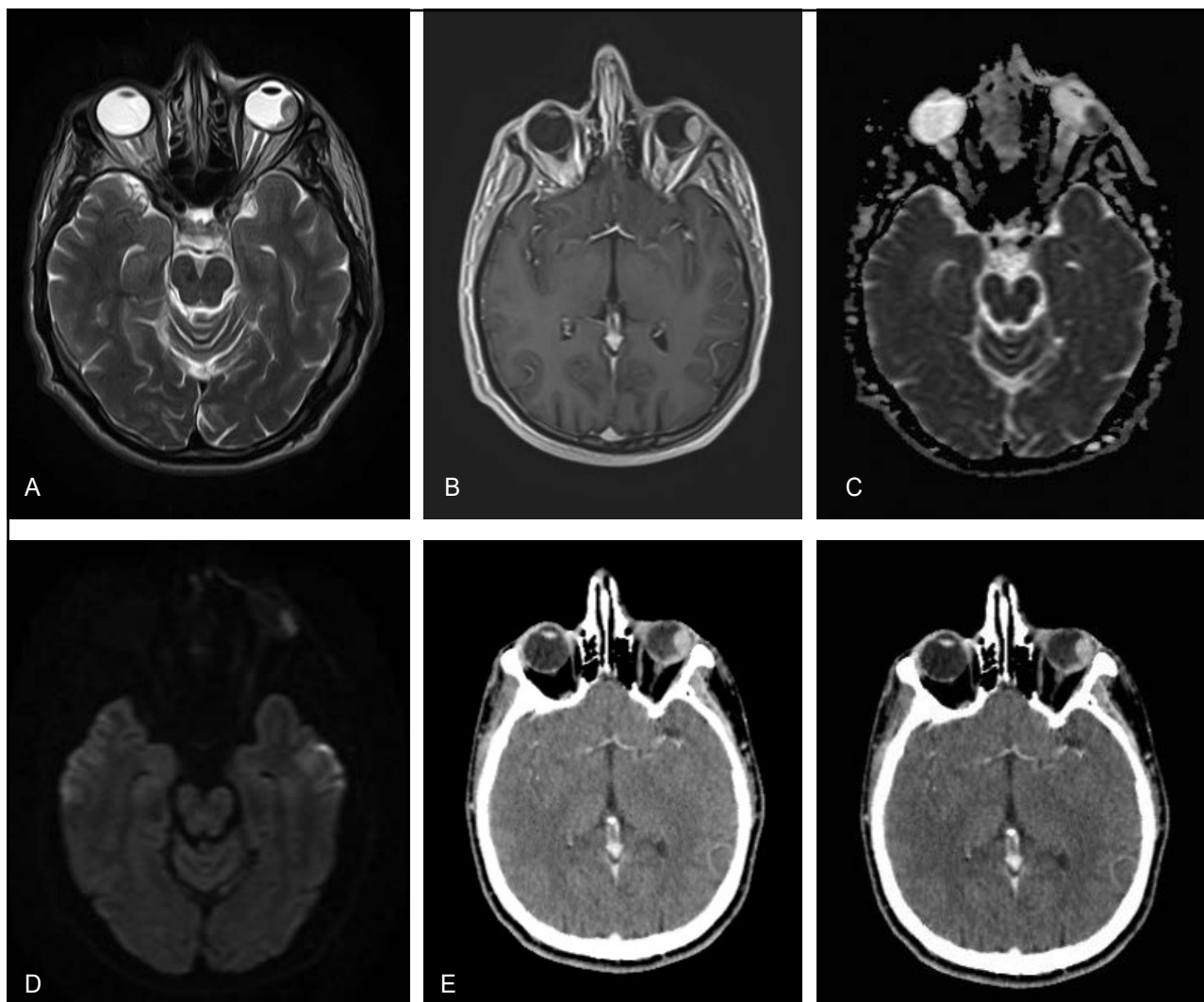| Uveal melanoma size	Before treatment	After treatment		Vitreous	Significance of difference, p
		1-2 months	11-12 months		
	1	2	3		
Small	1.05±0.04	1.24±0.05	1.49±0.05	2.63 ± 0.07	$P_{12}<0.01$ $P_{13}<0.01$
Moderate	0.85±0.04	1.02±0.05	1.18±0.05	2.67 ± 0.08	$P_{12}<0.01$ $P_{13}<0.01$
Large	0.56±0.03	0.76±0.04	0.92±0.05	2.59 ± 0.06	$P_{12}<0.01$ $P_{13}<0.01$
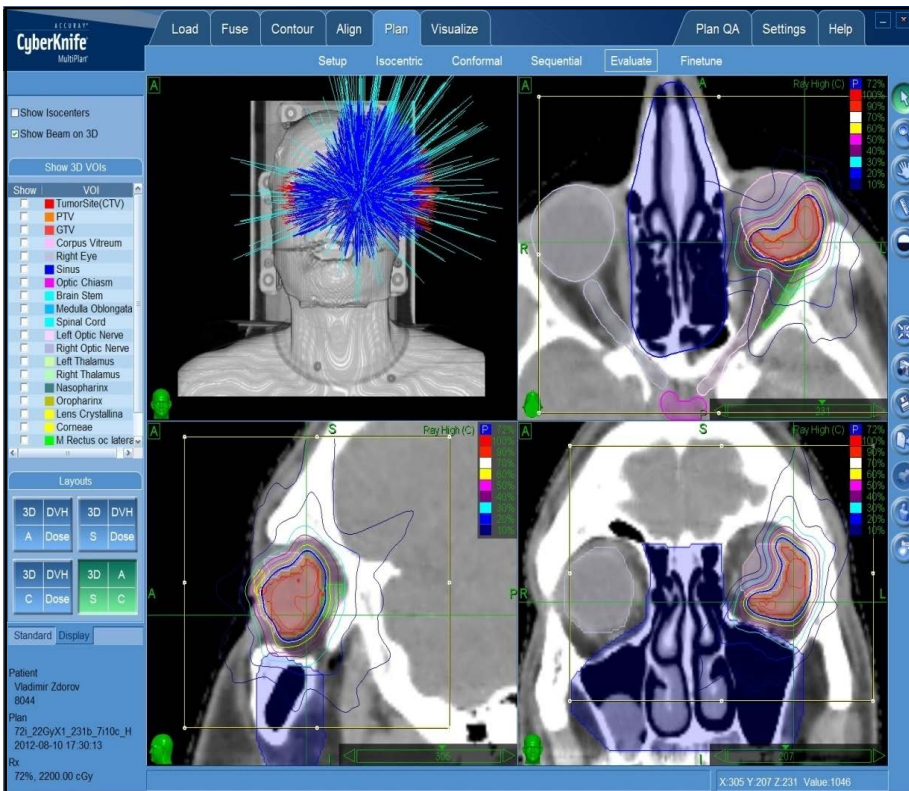
Fig. 1. CT-guided isodose planning for stereotactic radiosurgery with delineation of the critical structures of the eye like the lens, optic nerve and chiasm. Conformal 3D distribution of the dose to the tumor in the left orbit
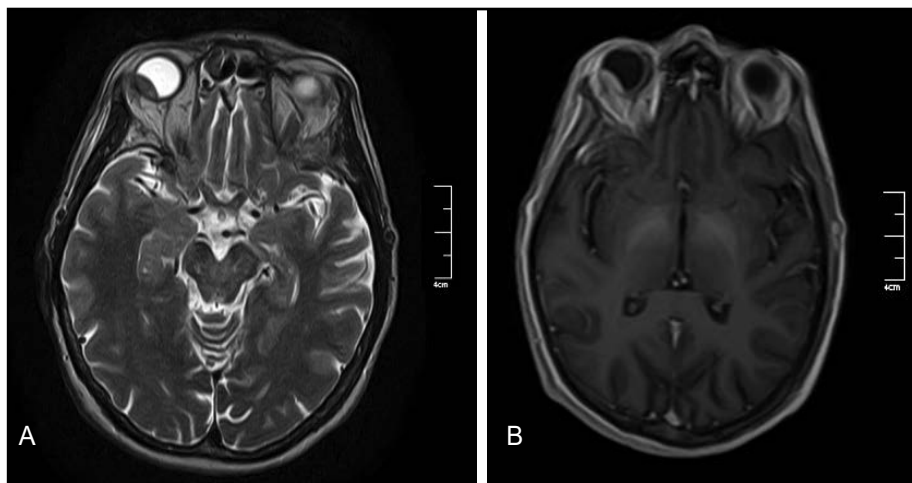
Fig. 2. Right-eye medium-sized (as per the classification system by Shields) uveal melanoma in patient B before treatment. Axial T2W MRI (A) shows a solitary hypointense intraocular mass in the inferior lateral quadrant of the right eye. On axial T1W image post paramagnetic contrast (B), the tumor demonstrates homogeneously increased signal intensity.
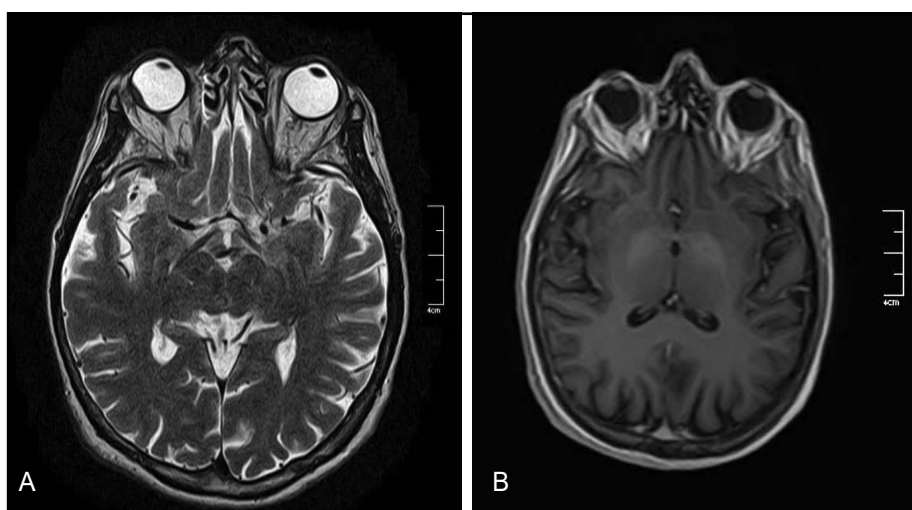
Fig. 3. Right-eye uveal melanoma in patient B two years after SRS treatment (20.0 Gy) for UM. Evidence of decreased tumor dimensions on axial T2W MRI (A). Axial T1W image post paramagnetic contrast (B) shows insubstantially increased signal from the tumor.

Fig. 4. Left-eye medium-sized (as per the classification system by Shields) uveal melanoma in patient Z before treatment. Axial T2W MRI (A) shows a solitary hypointense intraocular mass in the inferior lateral quadrant of the left eye. On axial T1W image post paramagnetic contrast (B), the tumor demonstrates substantially and homogeneously increased signal intensity. Diffusion-weighted image (C) demonstrates the hyperintense signal of the tumor. ADC image (D) demonstrates restricted diffusion with ADC = (0.74-0.81±0.0001) x10-3 mm2/s. On post-contrast CT (E), the tumor shows hyperdensity with active accumulation of the contrast medium.

Fig. 5. Left-eye uveal melanoma in patient Z two years after SRS treatment for UM (22.0 Gy). Evidence of decreased tumor dimensions on axial T2W MRI (A). Axial T1W image post paramagnetic contrast (B) shows insubstantially increased signal from the tumor. Diffusion-weighted image (C) demonstrates decreased hyperintensity of the tumor. ADC image (D) demonstrates increased ADC value (0.91-1.09±0.0001) x10^{-3} mm^2/s.